Physical Layer Security Performance Analysis for Relay-Aided Visible Light Communication System

Manjing Zhu, *Student Member, IEEE*, Yuhao Wang, *Senior Member, IEEE*, Xiaodong Liu, *Member, IEEE*, Zhengbao Qi, Xuanbang Chen, *Student Member, IEEE*, and Jin-Yuan Wang, *Member, IEEE*

***Abstract*—The risk of information leakage increases when the relay technology is introduced to extend the communication range and improve the quality of communication services of cell-edge users in visible light communication (VLC) systems. To evaluate these security risks, physical layer security (PLS) performance for decode-and-forward (DF) relay-aided VLC system is investigated in this paper. Specifically, the theoretical expressions of the upper and lower bounds of the security outage probability (SOP) for the DF relay-aided VLC system under the amplitude constraint are obtained based on a stochastic geometry analysis method. Monte Carlo simulation validates the correctness of the derived theoretical expressions of the upper and lower bounds of the SOP. Moreover, simulation results show that the security outage performance of the DF relay-aided VLC system is deteriorated compared with the non-relay VLC system. Furthermore, the influences of the eavesdroppers' distribution density, the radiation radius of LED source, the radiation radius and deployment height of the relay on the SOP have been investigated. Last but not least, the optimal deployment height of the relay can be determined for achieving the optimum security outage performance. These parameters can effectively guide the design of the secure relay-aided VLC system.**

***Index Terms*—Decode-and-forward, physical layer security, relay, security outage probability, visible light communication.**

Manuscript received 22 January 2023; revised 21 March 2023; accepted 26 March 2023. Date of publication 30 March 2023; date of current version 17 April 2023. This work was supported in part by the National Natural Science Foundation of China under Grant 62061030, in part by the Young Natural Science Foundation of Jiangxi Province under Grant 20224BAB212004, in part by the Education Department of Jiangxi Province through the Science and Technology Research Project under Grant GJJ2210601, in part by Jiangxi Open University through Science Research Project under Grants JKND2002 and JXKDJG-22-JWC-1, in part by the Natural Science Foundation of Jiangsu Province under Grant BK20221328, and in part by the open research fund of Key Lab of Broadband Wireless Communication and Sensor Network Technology, the Ministry of Education, China, under Grant JZNY202115. *(Corresponding authors: Yuhao Wang; Xiaodong Liu.)*

Manjing Zhu is with the School of Information Engineering, Nanchang University, Nanchang 330031, China, and also with the Modern Education Technology Center, Jiangxi Open University, Nanchang 330046, China (e-mail: zhumanjing@jxrtvu.com).

Yuhao Wang is with the School of Information Engineering, Nanchang University, Nanchang 330031, China, and also with the Shangrao Normal University, Shangrao 334001, China (e-mail: wangyuhao@ncu.edu.cn).

Xiaodong Liu is with the School of Information Engineering, Nanchang University, Nanchang 330031, China, and also with the Institut supérieur d'électronique de Paris, 75006 Paris, France (e-mail: xiaodongliu@whu.edu.cn).

Zhengbao Qi is with the United Testing Services (Jiangxi) Co., Ltd, Nanchang 330029, China (e-mail: qzb770725@163.com).

Xuanbang Chen is with the School of Information Engineering, Nanchang University, Nanchang 330031, China (e-mail: chenxuanbang@email.ncu.edu.cn).

Jin-Yuan Wang is with the Key Laboratory of Broadband Wireless Communication and Sensor Network Technology, Nanjing University of Posts and Telecommunications, Nanjing 210003, China (e-mail: jywang@njupt.edu.cn).

Digital Object Identifier 10.1109/JPHOT.2023.3263122

I. Introduction

With the explosive growth of various intelligent terminals, the exponentially increasing demands for mobile data traffic have brought severe challenge to radio frequency (RF) communication in terms of spectrum scarcity [1], [2]. Visible light communication (VLC) based on light-emitting diode (LED) can provide high-capacity, high-bandwidth communication services with its 400 THz license-free visible light spectrum resources [3], [4]. Thus, VLC is considered as an effective supplement technology to RF communication to alleviate the scarcity of spectrum resources. Moreover, due to the high reuse of visible light in space and frequency and weak wall penetration characteristic, VLC can be used to support high density and large scale user connection scenarios with certain security [5]. Existing research results show that VLC will become one of the strongest supporting technologies for future wireless communication networks [6]. However, the attenuation nature of the line-of-sight (LoS) link in the visible light transmission channel seriously restricts the communication range of the VLC cell [7].

Cooperative relay is proposed as an efficient technique in improving system connectivity and extending communication service coverage, especially for cell-edge users [8], [9]. Moreover, there are generally multiple LEDs with different configurations and deployment locations in an indoor scenario to satisfy various illumination requirements. Thus, it is very interesting to introduce the relay technology into VLC scenarios to unlock the nature advantage of multi-LEDs. And it can improve the communication service quality of the cell-edge users and enlarge communication service scope of the VLC system. Based on these advantages, there are some works focusing on relay-aided VLC systems. In [10], [11], [12], the authors are focused on orthogonal multiple access (OMA)-based VLC systems with the aid of relay nodes to improve the system connection reliability performance. Specifically, the authors in [10] investigated a relay-assisted VLC system based on direct current bias optical orthogonal frequency division multiplexing (DCO-OFDM), and derived the bit error rate (BER) performance. Also, it verified that the BER performance of decode-and-forward (DF) relaying system outperformed amplify-and-forward (AF) relaying system. In [12], the authors adopted adaptive physical layer network coding to boost the capacity of relay-assisted OFDM VLC networks. However, the spectrum of relay-aided VLC systems based on OMA technology is underutilized. Thus, the relay-aided VLC system based on non-orthogonal multiple

access (NOMA) has attracted a lot of attention [13], [14]. In [13], the authors proposed a hybrid VLC/RF cooperative relay network with NOMA, and the far user can adaptively choose either the hybrid VLC/RF relaying link or the direct VLC source link to decode information. In [14], the authors derived the theoretical expression of the outage probability for DF relay-aided VLC system with NOMA, and obtained 15 dB transmitting signal-to-noise ratio (SNR) gains in 10^{-3} outage probability level compared with the non-relay VLC system.

Relay-aided VLC systems can expand the scope of communication services to improve the quality of communication services for cell-edge users. However, visible light signal transmission still faces the risk of being eavesdropped due to the inhere broadcast nature of the visible light spectrum. Thus, physical layer security (PLS) as a promising technology in RF communication networks can be applied into VLC systems to enhance the security of the information transmission [15], [16], [17], [18]. First of all, the authors in [15] derived the upper and lower bounds of the secrecy capacity for indoor VLC wiretap channel under the amplitude constraint on transmission signals. Then, taking into account the randomness of eavesdroppers, the authors in [16] investigated a secure VLC system with randomly distributed terminals, and obtained the closed-form expressions of the security outage probability (SOP) and average security capacity by employing a stochastic geometry analysis method. To investigate the practical amplitude constraint instead of an average power constraint in the VLC system, the authors in [17] studied the security performance for the VLC system with multiple eavesdroppers under the amplitude constraint on the transmission signal, and derived the theoretical expressions for the upper and lower bounds of the SOP and the average secrecy capacity by using a stochastic geometry analysis method. Furthermore, the authors in [18] derived the upper and lower bounds on the secrecy capacity of single input single output VLC wiretap system based on multi-path reflections of the LoS link and the non-LoS link.

These above-mentioned works can provide abundant theoretical basis and meaningful insight for the PLS performance of VLC systems. However, compared with VLC systems, the relay-aided VLC system further increases security risks due to the introduction of relay nodes. To study the PLS performance of relay-aided VLC systems, the authors in [19] investigated the PLS performance for a hybrid VLC/RF system and derived the exact expressions of the SOP and the average security capacity in the presence of single legitimate receiver and single eavesdropper. Then, considering randomly distributed eavesdroppers, the authors in [20] studied the SOP of a hybrid VLC/RF system by employing a stochastic geometry analysis method. Moreover, taking into account the unknown channel state information (CSI), the authors in [21] investigated the PLS performance in a hybrid VLC/RF network based on both the known and unknown CSI and then evaluated the average secrecy capacity and secrecy outage probability performance. In conclusion, these works can provide numerous theoretical basis for studying the PLS performance of the hybrid VLC/RF cooperative relay system. However, the relay forwarding is achieved by the RF communication in these mentioned hybrid VLC/RF cooperative relay systems. Moreover, the relay, the legitimate user and the eavesdropper are located in the same plane. Thus, they can not be directly applied into the practical and pure relay-aided VLC systems with the relay, the legitimate user and multiple eavesdroppers being randomly distributed in different spatial planes. What's more, the transmission signals in VLC systems need to satisfy the requirements of non-negativity real values and the amplitude constraint [22]. Thus, the classic Shannon capacity can not be applied into the channel capacity calculation of the relay-aided VLC system.

Motivated by those facts, the PLS performance of the relay-aided VLC system is investigated with the relay located in a different spatial plane from multiple eavesdroppers and the legitimate user, and the corresponding influence factors are analyzed in this paper. At the same time, in order to focus on investigating the PLS performance of the relay-aided VLC system, DF relaying protocol is introduced directly due to the performance of DF relaying system exceeding AF relaying system [23]. Moreover, different from the works [19], [20], [21], the main contributions of this paper are summarized as follows.

1) Considering the practical deployment characteristic of multiple illumination LEDs in indoor scenarios and the demands of the transmission signal secure communication, the PLS performance of a pure relay-aided VLC system is investigated in this paper. Generally, multiple illumination LEDs are uniformly deployed in indoor different spatial planes to provide illumination services for cell-edge users. And the illumination LED closest to the legitimate cell-edge user is chosen as the relay to assist communication. At the same time, considering the random distribution properties of user terminals, it is assumed that multiple eavesdroppers follow random homogeneous poisson point process (HPPP) distribution and the legitimate user follows uniform distribution. Based on the non-negative real value characteristic and the practical amplitude constraint on the transmission signal in VLC systems, the probability density function (PDF) and the corresponding cumulative distribution function (CDF) of the received SNRs from eavesdroppers, the relay and the legitimate user are obtained by adopting a stochastic geometry analysis method.
2) Based on the upper and lower bounds of the security capacity, the theoretical expressions of the upper and lower bounds of the SOP are obtained for the considered DF relay-aided VLC system. Moreover, Mente Carlo simulation results verify the correctness of the theoretical expressions of the upper and lower bounds of the SOP. Furthermore, it proves that the security outage performance for the considered DF relay-aided VLC system is deteriorated compared with the non-relay VLC system. In addition, the corresponding impact factors of the SOP for the DF relay-aided VLC system are investigated from the eavesdroppers' distribution density, the radiation radius of LED source, the radiation radius and deployment height of the relay. It can be seen that there is an optimal deployment height of the relay to obtain the optimum security outage performance of the considered system. These parameters

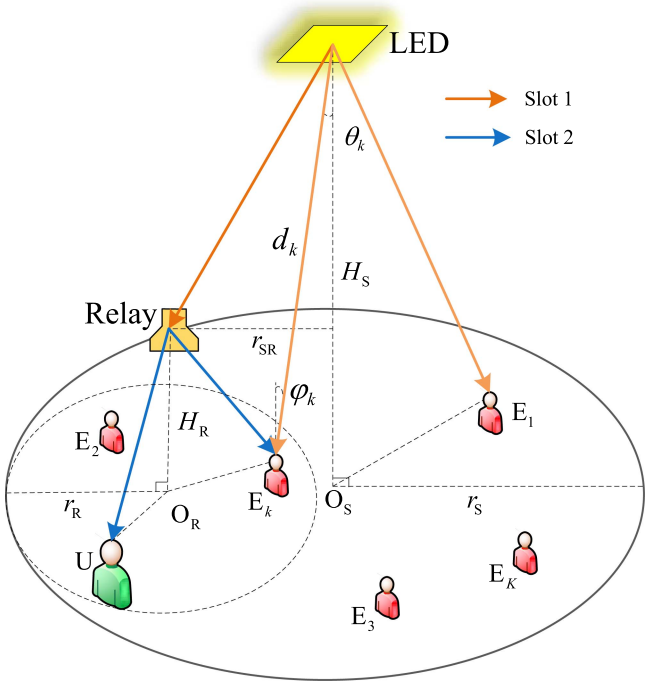

Fig. 1. DF relay-aided VLC system model.

can effectively guide the design of the secure relay-aided VLC system.

The rest of this paper is organized as follows. The considered system model and signal structure are introduced in Section II. Section III analyzes the SOP for the DF relay-aided VLC system. Simulation results are presented and discussed in Section IV. Finally, conclusions are drawn in Section V.

II. System Model

In this section, the considered system model and signal structure are presented to facilitate analysis. Then, the PDF and CDF of the received SNRs are obtained based on the stochastic geometry analysis method.

A. System Model

The considered indoor downlink DF relay-aided VLC system, which consists of a LED source (S), a relay (R), a legitimate user (U) and K eavesdroppers ($\mathrm{E}_k, 1 \le k \le K$), and each receiver (R, U, E_k) is equipped with a photodiode (PD), as shown in Fig. 1. Specifically, the LED source is located at the center of the ceiling with a height of H_S from the floor, and simultaneously provides illumination and communication services within its radiation radius r_S. In order to investigate the security performance of the legitimate user from the perspective of statistical probability, considering the user's mobile habits and similar to the works of [16] and [17], a legitimate user which is close to the relay is assumed to be distributed uniformly at a certain radiation edge cell of the LED source and the radiation area of the relay. Similar to [12], it is assumed that the legitimate user can not receive the signal transmitted from LED source due to the VLC channel attenuation or obstruction nature. In other words, the direct transmission link between the LED source and the legitimate cell-edge user is assumed to be absent. Considering multiple LED task lights with different configurations and deployment locations in an indoor scenario, a LED task light which is closest to the legitimate cell-edge user is chosen as the relay to assist communication between the LED source and the legitimate cell-edge user. The radiation radius and the deployment height from the floor of the relay are denoted as r_R and H_R, respectively. At the same time, according to previous research results that the performance of DF relaying system is superior to AF relaying system [23], DF relaying protocol is adopted directly in the considered relay-aided VLC system. Therefore, the signal transmission process is that the relay firstly receives the transmitted signal from the LED source, and then decodes and forwards signals to the legitimate user by employing the DF relaying protocol.

In the practical VLC scenarios, the locations and numbers of the eavesdroppers are usually unknown [24]. HPPP can describe a random location distribution model with different numbers of eavesdroppers [16], [17]. To analyze comprehensively the legitimate user's security performance under the condition of different numbers and random locations of eavesdroppers, it is assumed that the eavesdroppers follow a HPPP distribution in the service area. Also, the eavesdroppers always try to eavesdrop transmission signals on the SR and RU links. Note that the SR link is between the LED source and the relay, and the RU link is between the relay and the legitimate user. Therefore, the eavesdroppers' HPPP distribution can be modeled as

$$\mathcal{P}(N=k)=\frac{\mu^k \exp(-\mu)}{k!}, \tag{1}$$

where N denotes the number of eavesdroppers, and k ($k = 0, 1, \ldots, K$) is a sample value of N. $\mu = \lambda\pi D^2$ is the mean of the HPPP, and the corresponding λ and D denote the HPPP distribution density and distribution radius of the eavesdroppers, respectively. Specifically, the eavesdropper's distribution radius is $D = r_\mathrm{S}$ in the LED source radiating cell and $D = r_\mathrm{R}$ in the relay radiating cell, respectively. The PDF of the horizontal distance between the eavesdroppers and the LED source or the relay can be given as $f_r = \lambda/\mu = 1/(\pi D^2)$.

In VLC systems, there co-exist LoS and non-LoS links between the transmitter and the receiver. Since the VLC channel is dominated by the LoS link [25], the LoS link is considered and the non-LoS link is neglected in this paper. Thus, the channel gain $h_{i,j}$ from the transmitter i to the receiver j can be given as [26]

$$h_{i,j}=\frac{(m_{t,i,j}+1)A_{\mathrm{PD},i,j}}{2\pi d_{i,j}^2}\cos^{m_{t,i,j}}(\theta_{i,j})g(\varphi_{i,j})T(\varphi_{i,j})\cos\varphi_{i,j}, \tag{2}$$

where $i \in \{\mathrm{S}, \mathrm{R}\}$, $j \in \{\mathrm{R}, \mathrm{U}, \mathrm{E}_k\}$. $A_{\mathrm{PD},i,j}$ and $d_{i,j}$ represent the detection area of the j-th receiver PD and the Euclidean distance between the transmitter i and the receiver j, respectively. $\varphi_{i,j}$

and $\theta_{i,j}$ denote the incident angle and radiation angle, respectively. $m_{t,i,j}$ is the Lambertian emission order and can be calculated by $m_{t,i,j}=-\ln 2/\ln(\cos\theta_{1/2,i,j})$, and the corresponding $\theta_{1/2,i,j}$ is LED semi-angle. $g(\varphi_{i,j})=n_{i,j}^2/\sin^2(\Psi_{i,j}),(0\leq\varphi_{i,j}\leq\Psi_{i,j})$ is the optical concentrator gain, and it depends on the refractive index $n_{i,j}$ of the optical concentrator and the field of view $\Psi_{i,j}$ of the receiver PD. $T(\varphi_{i,j})$ represents the optical filter gain. Note that $h_{i,j}=0$ when $\varphi_{i,j}>\Psi_{i,j}$.

In order to effectively employ the statistical information of all receivers' locations, similar to the works in [16] and [17], the relationship between the received power $P_{i,j}$ of the relay or user terminals and the distance $d_{i,j}$ from the transmitter to the receiver can be given as

$$P_{i,j}=C_{\mathrm{VLC},i,j}P_i^2G_{t,i,j}^2G_{r,i,j}^2/d_{i,j}^4, \tag{3}$$

where $C_{\mathrm{VLC},i,j}=7.8\times10^3(\mathrm{cm}^2\cdot\mathrm{mW})^2$ is the power constant at the receiver, which is related to the optical-to-electrical conversion efficiency and optical power constant. $G_{t,i,j}^2=\cos^{m_{t,i,j}}(\theta_{i,j})$ and $G_{r,i,j}^2=\cos^{m_{r,i,j}}(\varphi_{i,j})$ are the radiation gain of the transmitter LED and the incidence gain of the receiver PD, respectively. And $m_{r,i,j}=-\ln 2/\ln(\cos\Psi_{i,j})$. P_i denotes the transmitting power of the transmitter.

In this paper, all receivers are assumed to try to acquire the best performance for their perspective. Thus, the incidence line is always perpendicular to the PD axis at each receiver, i.e., $G_{r,i,j}^2=1$. Moreover, based on the geometric relationship in Fig. 1, $d_{i,j}=\sqrt{H_{i,j}^2+r_{i,j}^2}$ and $\cos(\theta_{i,j})=H_{i,j}/\sqrt{H_{i,j}^2+r_{i,j}^2}$ can be obtained, where $H_{i,j}$ and $r_{i,j}$ denote the perpendicular distance and horizontal distance between the transmitter i and the receiver j, respectively. Moreover, the VLC channel gain is essentially effected by distance. Thus, the relationship between the received power $P_{i,j}$ of the relay or user terminals and the distance can be rewritten as

$$P_{i,j}=C_{\mathrm{VLC},i,j}P_i^2H_{i,j}^{2m_{t,i,j}}\left(H_{i,j}^2+r_{i,j}^2\right)^{-2-m_{t,i,j}}. \tag{4}$$

B. Signal Structure

In the DF relay-aided VLC system, the signal transmission process includes two slots, i.e., LED source transmits signals to the relay and the relay forwards signals to the legitimate user. In the first slot, LED source transmits signals to the relay. The signal transmitted from the LED source can be given as

$$x_{\mathrm{ST}}=\sqrt{P_{\mathrm{S}}}x_{\mathrm{S}}+I_{\mathrm{DC}}, \tag{5}$$

where P_{S} is the electrical alternating current power of LED source. x_{S} represents the transmitted signal from LED source. Moreover, x_{S} is assumed to follow unit variance and satisfy an amplitude constraint, i.e., $|x_{\mathrm{S}}|\leq\mathcal{A}$. Note that $\mathcal{A}$ $(\mathcal{A}>0)$ is a constant [27]. $I_{\mathrm{DC}}\in[I_{\mathrm{L}},I_{\mathrm{H}}]$ is DC bias offset and is added to the source LED to satisfy the non-negative requirement of transmission signals in the considered DF relay-aided VLC system, and the corresponding I_{L} and I_{H} are the minimum and maximum input DC bias offset in the source LED linear region, respectively. To avoid harmonic distortion by the nonlinearity of the LED, the signal input to the LED must be restrained within the linear region of the LED [28]. Thus, the signal amplitude $\mathcal{A}$ satisfies

$$\mathcal{A}\leq\min\left(I_{\mathrm{DC}}-I_{\mathrm{L}},I_{\mathrm{H}}-I_{\mathrm{DC}}\right). \tag{6}$$

Thus, the received electrical signals by the relay and the k-th eavesdropper after removing the DC component can be respectively given as

$$y_{\mathrm{SR}}=\eta h_{\mathrm{SR}}\sqrt{P_{\mathrm{S}}}x_{\mathrm{S}}+n_{\mathrm{SR}}, \tag{7a}$$

$$y_{\mathrm{SE}_k}=\eta h_{\mathrm{SE}_k}\sqrt{P_{\mathrm{S}}}x_{\mathrm{S}}+n_{\mathrm{SE}_k}, \tag{7b}$$

where η denotes the optical-to-electrical conversion efficiency. $n_{\mathrm{SR}}\sim\mathcal{CN}(0,\mathcal{N}_{\mathrm{SR}})$ and $n_{\mathrm{SE}_k}\sim\mathcal{CN}(0,\mathcal{N}_{\mathrm{SE}_k})$ denote the additive white Gaussian noise in the SR link and the SE_k link, respectively. $\mathcal{N}_{\mathrm{SR}}$ and $\mathcal{N}_{\mathrm{SE}_k}$ are the corresponding noise variance, respectively.

Then, according to (4), the received SNRs at the relay and the k-th eavesdropper in the first slot are respectively given as

$$\gamma_{\mathrm{SR}}=\mathcal{C}_{\mathrm{SR}}\left(H_{\mathrm{SR}}^2+r_{\mathrm{SR}}^2\right)^{(-2-m_{t,\mathrm{SR}})}, \tag{8a}$$

$$\gamma_{\mathrm{SE}_k}=\mathcal{C}_{\mathrm{SE}_k}\left(H_{\mathrm{SE}_k}^2+r_{\mathrm{SE}_k}^2\right)^{(-2-m_{t,\mathrm{SE}_k})}, \tag{8b}$$

where $\mathcal{C}_{\mathrm{SR}}=C_{\mathrm{VLC,SR}}P_{\mathrm{S}}^2H_{\mathrm{SR}}^{2m_{t,\mathrm{SR}}}/\mathcal{N}_{\mathrm{SR}}$, and $\mathcal{C}_{\mathrm{SE}_k}=C_{\mathrm{VLC,SE}_k}P_{\mathrm{S}}^2H_{\mathrm{SE}_k}^{2m_{t,\mathrm{SE}_k}}/\mathcal{N}_{\mathrm{SE}_k}$.

In the second slot, the relay decodes and forwards signals to the legitimate user by employing DF relaying protocol. Meantime, eavesdroppers try to wiretap the transmission signals in the RU link. Taking into account the instantaneity of the delay in the decoding and forwarding process, similar to the works in [14] and [29], the instantaneous delay in the relay-aided VLC system can be ignored. Thus, the received electrical signals by the legitimate user and the k-th eavesdropper after removing the DC component in the second slot can be given as

$$y_{\mathrm{RU}}=\eta h_{\mathrm{RU}}\sqrt{P_{\mathrm{R}}}x_{\mathrm{R}}+n_{\mathrm{RU}}, \tag{9a}$$

$$y_{\mathrm{RE}_k}=\eta h_{\mathrm{RE}_k}\sqrt{P_{\mathrm{R}}}x_{\mathrm{R}}+n_{\mathrm{RE}_k}, \tag{9b}$$

where P_{R} and x_{R} denote the transmitting power of the relay and the forwarded signal by the relay, respectively. $n_{\mathrm{RU}}\sim\mathcal{CN}(0,\mathcal{N}_{\mathrm{RU}})$ and $n_{\mathrm{RE}_k}\sim\mathcal{CN}(0,\mathcal{N}_{\mathrm{RE}_k})$ denote the additive white Gaussian noise in the RU link and the RE_k link, respectively. $\mathcal{N}_{\mathrm{RU}}$ and $\mathcal{N}_{\mathrm{RE}_k}$ are the corresponding noise variance, respectively.

Similarly, according to (4), the received SNRs at the legitimate user and the k-th eavesdropper in the second slot are respectively given as

$$\gamma_{\mathrm{RU}}=\mathcal{C}_{\mathrm{RU}}\left(H_{\mathrm{RU}}^2+r_{\mathrm{RU}}^2\right)^{(-2-m_{t,\mathrm{RU}})}, \tag{10a}$$

$$\gamma_{\mathrm{RE}_k}=\mathcal{C}_{\mathrm{RE}_k}\left(H_{\mathrm{RE}_k}^2+r_{\mathrm{RE}_k}^2\right)^{(-2-m_{t,\mathrm{RE}_k})}, \tag{10b}$$

where $\mathcal{C}_{\mathrm{RU}}=C_{\mathrm{VLC,RU}}P_{\mathrm{R}}^2H_{\mathrm{RU}}^{2m_{t,\mathrm{RU}}}/\mathcal{N}_{\mathrm{RU}}$ and $\mathcal{C}_{\mathrm{RE}_k}=C_{\mathrm{VLC,RE}_k}P_{\mathrm{R}}^2H_{\mathrm{RE}_k}^{2m_{t,\mathrm{RE}_k}}/\mathcal{N}_{\mathrm{RE}_k}$.

Therefore, the received SNRs of the receiver j from the transmitter i at the first or the second slot is summarized as

$$\gamma_{i,j}=\mathcal{C}_{i,j}\left(H_{i,j}^2+r_{i,j}^2\right)^{(-2-m_{t,i,j})}, \tag{11}$$

where $\mathcal{C}_{i,j} = C_{\mathrm{VLC},i,j} P_i^2 H_{i,j}^{2m_{t,i,j}} / \mathcal{N}_{i,j}$, and $\mathcal{N}_{i,j}$ denotes the corresponding noise variance.

Due to the amplitude constraint on transmission signals in the practical VLC systems, according to the work in [15], the upper and lower bounds of the security capacity in VLC channel can be respectively given as

$$C_{\mathrm{sec}}^{\mathrm{u}}\left(\gamma_{i,j'}, \gamma_{i,\mathrm{E}}^{\max}\right) = \max\left\{\frac{1}{2}\log_2\frac{\gamma_{i,j'}+1}{\gamma_{i,\mathrm{E}}^{\max}+1}, 0\right\}, \tag{12a}$$

$$C_{\mathrm{sec}}^{\mathrm{l}}\left(\gamma_{i,j'}, \gamma_{i,\mathrm{E}}^{\max}\right) = \max\left\{\frac{1}{2}\log_2\frac{6\gamma_{i,j'}+3\pi e}{\pi e\gamma_{i,\mathrm{E}}^{\max}+3\pi e}, 0\right\}, \tag{12b}$$

where $i \in \{\mathrm{S}, \mathrm{R}\}$, $j' \in \{\mathrm{R}, \mathrm{U}\}$. The superscript u and l denote respectively the upper and lower bounds to facilitate analysis. $\gamma_{i,\mathrm{E}}^{\max} = \max_{1\le k\le K}\{\gamma_{i,\mathrm{E}_k}\}$ denotes the highest received SNR among all eavesdroppers. Note that in the first slot, the received SNR by the relay and the highest received SNR among all eavesdroppers are γ_{SR} and $\gamma_{\mathrm{SE}}^{\max}$, respectively. In the second slot, the received SNR by the legitimate user and the highest received SNR among all eavesdroppers are γ_{RU} and $\gamma_{\mathrm{RE}}^{\max}$, respectively.

By employing $f_r = 1/(\pi D^2)$, the CDF of the horizontal distance $r_{i,j}$ between the transmitter i and the receiver j can be derived as

$$P(x) = \int_0^{2\pi}\int_0^{x}\frac{1}{\pi D^2} r dr d\theta = \frac{x^2}{D^2}. \tag{13}$$

Then, the PDF of the horizontal distance $r_{i,j}$ can be obtained as $f(x) = 2x/D^2$, $(0 \le x \le D)$, which is suitable for the relay, the legitimate user and eavesdroppers. Further, by utilizing the stochastic geometry analysis method, the PDF and the corresponding CDF of the received SNR $\gamma_{i,j}$ can be respectively achieved as

$$f_{\gamma_{i,j}}(x) = a_{i,j}x^{b_{i,j}}, \tag{14a}$$

$$F_{\gamma_{i,j}}(x) = a_{i,j}x^{c_{i,j}}/c_{i,j} + \Theta_{i,j}, \tag{14b}$$

where $a_{i,j} = -c_{i,j}/(r_{i,j}^2 \mathcal{C}_{i,j}^{c_{i,j}})$, $b_{i,j} = c_{i,j} - 1$, $c_{i,j} = -1/(m_{t,i,j}+2)$ and $\Theta_{i,j} = H_{i,j}^2/r_{i,j}^2 + 1$. The variable $x \in [\gamma_{i,j,\min}, \gamma_{i,j,\max}]$, and the corresponding $\gamma_{i,j,\min} = \mathcal{C}_{i,j}(H_{i,j}^2 + r_{i,j}^2)^{(-2-m_{t,i,j})}$ and $\gamma_{i,j,\max} = \mathcal{C}_{i,j}H_{i,j}^{(-4-2m_{t,i,j})}$.

Because the variables γ_{i,E_k} $(1 \le k \le K)$ are mutually independent and $\gamma_{i,\mathrm{E}}^{\max} = \max_{1\le k\le K}\{\gamma_{i,\mathrm{E}_k}\}$, by using the statistical probability theory, the CDF of $\gamma_{i,\mathrm{E}}^{\max}$ can be obtained as

$$F_{\gamma_{i,\mathrm{E}}^{\max}}(x) = \prod_{k=1}^{K} F_{\gamma_{i,\mathrm{E}_k}}(x). \tag{15}$$

Thus, the PDF of $\gamma_{i,\mathrm{E}}^{\max}$ can be given as

$$\begin{aligned} f_{\gamma_{i,\mathrm{E}}^{\max}}(x) &= a_{i,\mathrm{E}}K\sum_{k=0}^{K-1}\mathrm{Q}\left(\frac{a_{i,\mathrm{E}}}{c_{i,\mathrm{E}}}\right)^k x^{c_{i,\mathrm{E}}k+c_{i,\mathrm{E}}-1}\Theta_{i,\mathrm{E}}^{K-1-k} \\ &= a_{i,\mathrm{E}}K\sum_{k=0}^{K-1}\alpha_k x^{\beta_k}, \end{aligned} \tag{16}$$

where $\mathrm{Q} = \binom{K-1}{k}$ is a statistical combination. To simplify the above expression, α_k and β_k are used to replace $\mathrm{Q}\left(\frac{a_{i,\mathrm{E}}}{c_{i,\mathrm{E}}}\right)^k \Theta_{i,\mathrm{E}}^{K-1-k}$ and $c_{i,\mathrm{E}}k + c_{i,\mathrm{E}} - 1$, respectively. Namely, $\alpha_k = \mathrm{Q}\left(\frac{a_{i,\mathrm{E}}}{c_{i,\mathrm{E}}}\right)^k \Theta_{i,\mathrm{E}}^{K-1-k}$ and $\beta_k = c_{i,\mathrm{E}}k + c_{i,\mathrm{E}} - 1$.

III. Security Outage Probability Analysis

In this section, the upper and lower bounds of the SOP in the SR and RU links are derived, and then the upper and lower bounds of the SOP in the whole link from the LED source to the legitimate user in the DF relay-aided VLC system are obtained. Moreover, the upper and lower bounds of the SOP in the non-relay VLC system are also obtained for comparison.

Firstly, according to the upper and lower bounds of the secure capacity in (12), the upper and lower bounds of the SOP in the SR link can be respectively expressed as

$$\begin{aligned} P_{\mathrm{SOP}}^{\mathrm{SR,u}} &= \mathbb{P}\left(C_{\mathrm{sec}}^{\mathrm{l}} \le C_{\mathrm{th}}\right) = \mathbb{P}\left(\gamma_{\mathrm{SR}} \le \sigma_{\mathrm{u}}\gamma_{\mathrm{SE}}^{\max} + \zeta_{\mathrm{u}}\right) \\ &= \int_{y_{\min}}^{y_{\max}}\int_{x_{\min}}^{x_{\max}} f_{\gamma_{\mathrm{SR}}}(x) f_{\gamma_{\mathrm{SE}}^{\max}}(y) dxdy, \end{aligned} \tag{17a}$$

$$\begin{aligned} P_{\mathrm{SOP}}^{\mathrm{SR,l}} &= \mathbb{P}\left(C_{\mathrm{sec}}^{\mathrm{u}} \le C_{\mathrm{th}}\right) = \mathbb{P}\left(\gamma_{\mathrm{SR}} \le \sigma_{\mathrm{l}}\gamma_{\mathrm{SE}}^{\max} + \zeta_{\mathrm{l}}\right) \\ &= \int_{y_{\min}}^{y_{\max}}\int_{x_{\min}}^{x_{\max}} f_{\gamma_{\mathrm{SR}}}(x) f_{\gamma_{\mathrm{SE}}^{\max}}(y) dxdy, \end{aligned} \tag{17b}$$

where $\sigma_{\mathrm{u}} = \pi e 2^{2C_{\mathrm{th}}}/6$, $\zeta_{\mathrm{u}} = 3\sigma_{\mathrm{u}} - \pi e/2$, $\sigma_{\mathrm{l}} = 2^{2C_{\mathrm{th}}}$ and $\zeta_{\mathrm{l}} = \sigma_{\mathrm{l}} - 1$, and the corresponding C_{th} denotes the security capacity threshold. Note that the superscript or subscript u and l denote respectively the upper bound and the lower bound. And u and l are omitted in the following discussion due to the similarity for the upper and lower bounds.

It can be seen that it is difficult to calculate the integrals of (17). To calculate (17), the integral upper and lower limits $x_{\max}$, $x_{\min}$, $y_{\max}$, and $y_{\min}$ need to be determined. Firstly, $x \in [\gamma_{\mathrm{SR,min}}, \gamma_{\mathrm{SR,max}}]$ and $y \in [\gamma_{\mathrm{SE,min}}, \gamma_{\mathrm{SE,max}}]$ can be obtained from (14). Then, $\gamma_{\mathrm{SR,max}}$ and $\gamma_{\mathrm{SE,min}}$ need to be respectively compared with $\sigma y + \zeta$ and $\gamma_{\mathrm{SE,limit}} = (\gamma_{\mathrm{SE,max}} - \zeta)/\sigma$ to determine the integral intervals. Therefore, the integral intervals are discussed as the following four cases.

Case 1, when $\sigma y + \zeta > \gamma_{\mathrm{SR,max}}$ and $\gamma_{\mathrm{SE,limit}} > \gamma_{\mathrm{SE,min}}$, there are $x \in [\gamma_{\mathrm{SR,min}}, \gamma_{\mathrm{SR,max}}]$ and $y \in [\gamma_{\mathrm{SE,limit}}, \gamma_{\mathrm{SE,max}}]$. According to the PDFs of the received SNRs, the upper and lower bounds of the SOP for case 1 in the SR link can be derived as

$$\begin{aligned} P_{\mathrm{SOP1}}^{\mathrm{SR}} &= \int_{\gamma_{\mathrm{SE,limit}}}^{\gamma_{\mathrm{SE,max}}}\int_{\gamma_{\mathrm{SR,min}}}^{\gamma_{\mathrm{SR,max}}} f_{\gamma_{\mathrm{SR}}}(x) f_{\gamma_{\mathrm{SE}}^{\max}}(y) dxdy \\ &= a_{\mathrm{SR}}a_{\mathrm{SE}}K\sum_{k=0}^{K-1}\alpha_k \int_{\gamma_{\mathrm{SE,limit}}}^{\gamma_{\mathrm{SE,max}}} y^{\beta_k}\int_{\gamma_{\mathrm{SR,min}}}^{\gamma_{\mathrm{SR,max}}} x^{b_{\mathrm{SR}}} dxdy \\ &= \Delta_{\mathrm{SR}}\sum_{k=0}^{K-1}\alpha_k\left(\gamma_{\mathrm{SR,max}}^{b_{\mathrm{SR}}+1} - \gamma_{\mathrm{SR,min}}^{b_{\mathrm{SR}}+1}\right)\frac{\gamma_{\mathrm{SE,max}}^{\beta_k+1} - \gamma_{\mathrm{SE,limit}}^{\beta_k+1}}{\beta_k+1}, \end{aligned} \tag{18}$$

where $\Delta_{\mathrm{SR}} = (a_{\mathrm{SR}}a_{\mathrm{SE}}K)/(b_{\mathrm{SR}}+1)$. α_k and β_k are the corresponding parameters for the SE link between the LED source and the eavesdropper with the highest received SNR among all eavesdroppers.

Case 2, when $\sigma y + \zeta > \gamma_{\mathrm{SR,max}}$ and $\gamma_{\mathrm{SE,limit}} < \gamma_{\mathrm{SE,min}}$, there are $x \in [\gamma_{\mathrm{SR,min}}, \gamma_{\mathrm{SR,max}}]$ and $y \in [\gamma_{\mathrm{SE,min}}, \gamma_{\mathrm{SE,max}}]$. Thus, the

upper and lower bounds of the SOP for case 2 in the SR link can be derived as

$$\begin{aligned} P_{\mathrm{SOP2}}^{\mathrm{SR}} &= \int_{\gamma_{\mathrm{SE,min}}}^{\gamma_{\mathrm{SE,max}}} \int_{\gamma_{\mathrm{SR,min}}}^{\gamma_{\mathrm{SR,max}}} f_{\gamma_{\mathrm{SR}}}(x) f_{\gamma_{\mathrm{SE}}^{\max}}(y) dxdy \\ &= a_{\mathrm{SR}} a_{\mathrm{SE}} K \sum_{k=0}^{K-1} \alpha_k \int_{\gamma_{\mathrm{SE,min}}}^{\gamma_{\mathrm{SE,max}}} y^{\beta_k} \int_{\gamma_{\mathrm{SR,min}}}^{\gamma_{\mathrm{SR,max}}} x^{b_{\mathrm{SR}}} dxdy \\ &= \Delta_{\mathrm{SR}} \sum_{k=0}^{K-1} \alpha_k \left(\gamma_{\mathrm{SR,max}}^{b_{\mathrm{SR}}+1} - \gamma_{\mathrm{SR,min}}^{b_{\mathrm{SR}}+1} \right) \frac{\gamma_{\mathrm{SE,max}}^{\beta_k+1} - \gamma_{\mathrm{SE,min}}^{\beta_k+1}}{\beta_k+1}. \end{aligned} \tag{19}$$

Case 3, when $\sigma y + \zeta < \gamma_{\mathrm{SR,max}}$ and $\gamma_{\mathrm{SE,limit}} < \gamma_{\mathrm{SE,min}}$, there is $x \in [\gamma_{\mathrm{SR,min}}, \sigma y + \zeta]$. However, $y_{\min}$ and $y_{\max}$ are empty set. Thus, the upper and lower bounds of the SOP in the SR link for case 3 are zero.

Case 4, when $\sigma y + \zeta < \gamma_{\mathrm{SR,max}}$ and $\gamma_{\mathrm{SE,limit}} > \gamma_{\mathrm{SE,min}}$, there are $x \in [\gamma_{\mathrm{SR,min}}, \sigma y + \zeta]$ and $y \in [\gamma_{\mathrm{SE,min}}, \gamma_{\mathrm{SE,limit}}]$. In case 4, the integrals of (17) are so complicated that the hypergeometric function $\mathrm{H}(\cdot)$ [30] needs to be introduced to calculate. Therefore, the upper and lower bounds of the SOP in the SR link for case 4 can be derived as

$$\begin{aligned} P_{\mathrm{SOP4}}^{\mathrm{SR}} &= \int_{\gamma_{\mathrm{SE,min}}}^{\gamma_{\mathrm{SE,limit}}} \int_{\gamma_{\mathrm{SR,min}}}^{\sigma y+\zeta} f_{\gamma_{\mathrm{SR}}}(x) f_{\gamma_{\mathrm{SE}}^{\max}}(y) dxdy \\ &= -\gamma_{\mathrm{SR,min}}^{b_{\mathrm{SR}}+1} \Delta_{\mathrm{SR}} \sum_{k=0}^{K-1} \alpha_k \int_{\gamma_{\mathrm{SE,min}}}^{\gamma_{\mathrm{SE,limit}}} y^{\beta_k} dy \\ &\quad + \sigma^{b_{\mathrm{SR}}+1} \Delta_{\mathrm{SR}} \sum_{k=0}^{K-1} \alpha_k \int_{\gamma_{\mathrm{SE,min}}}^{\gamma_{\mathrm{SE,limit}}} y^{\beta_k} \left(y + \frac{\zeta}{\sigma} \right)^{b_{\mathrm{SR}}+1} dy \\ &= -\gamma_{\mathrm{SR,min}}^{b_{\mathrm{SR}}+1} \Delta_{\mathrm{SR}} \sum_{k=0}^{K-1} \alpha_k \left(\frac{\gamma_{\mathrm{SE,limit}}^{\beta_k+1}}{\beta_k+1} - \frac{\gamma_{\mathrm{SE,min}}^{\beta_k+1}}{\beta_k+1} \right) \\ &\quad + \sigma^{b_{\mathrm{SR}}+1} \Delta_{\mathrm{SR}} \sum_{k=0}^{K-1} \alpha_k \\ &\quad \times \left[\frac{\delta^{b_{\mathrm{SR}}+1} \gamma_{\mathrm{SE,limit}}^{\beta_k+1} \mathrm{H}\left([-b_{\mathrm{SR}}-1, \beta_k+1], \beta_k+2, -\frac{\gamma_{\mathrm{SE,limit}}}{\delta} \right)}{\beta_k+1} \right. \\ &\quad \left. - \frac{\delta^{b_{\mathrm{SR}}+1} \gamma_{\mathrm{SE,min}}^{\beta_k+1} \mathrm{H}\left([-b_{\mathrm{SR}}-1, \beta_k+1], \beta_k+2, -\frac{\gamma_{\mathrm{SE,min}}}{\delta} \right)}{\beta_k+1} \right], \end{aligned} \tag{20}$$

where $\delta = \zeta/\sigma$. Thus, taking into account the above four case, the upper and lower bounds of the SOP in the SR link can be respectively summarized as

$$P_{\mathrm{SOP}}^{\mathrm{SR,u}} = P_{\mathrm{SOP1}}^{\mathrm{SR}}(\sigma_{\mathrm{u}}, \zeta_{\mathrm{u}}) + P_{\mathrm{SOP2}}^{\mathrm{SR}}(\sigma_{\mathrm{u}}, \zeta_{\mathrm{u}}) + P_{\mathrm{SOP4}}^{\mathrm{SR}}(\sigma_{\mathrm{u}}, \zeta_{\mathrm{u}}), \tag{21a}$$

$$P_{\mathrm{SOP}}^{\mathrm{SR,l}} = P_{\mathrm{SOP1}}^{\mathrm{SR}}(\sigma_{\mathrm{l}}, \zeta_{\mathrm{l}}) + P_{\mathrm{SOP2}}^{\mathrm{SR}}(\sigma_{\mathrm{l}}, \zeta_{\mathrm{l}}) + P_{\mathrm{SOP4}}^{\mathrm{SR}}(\sigma_{\mathrm{l}}, \zeta_{\mathrm{l}}). \tag{21b}$$

Similarly, the upper and lower bounds of the SOP in the RU link can be respectively summarized as

$$P_{\mathrm{SOP}}^{\mathrm{RU,u}} = P_{\mathrm{SOP1}}^{\mathrm{RU}}(\sigma_{\mathrm{u}}, \zeta_{\mathrm{u}}) + P_{\mathrm{SOP2}}^{\mathrm{RU}}(\sigma_{\mathrm{u}}, \zeta_{\mathrm{u}}) + P_{\mathrm{SOP4}}^{\mathrm{RU}}(\sigma_{\mathrm{u}}, \zeta_{\mathrm{u}}), \tag{22a}$$

$$P_{\mathrm{SOP}}^{\mathrm{RU,l}} = P_{\mathrm{SOP1}}^{\mathrm{RU}}(\sigma_{\mathrm{l}}, \zeta_{\mathrm{l}}) + P_{\mathrm{SOP2}}^{\mathrm{RU}}(\sigma_{\mathrm{l}}, \zeta_{\mathrm{l}}) + P_{\mathrm{SOP4}}^{\mathrm{RU}}(\sigma_{\mathrm{l}}, \zeta_{\mathrm{l}}). \tag{22b}$$

TABLE I
SIMULATION PARAMETERS

Parameter name	Value
Height from LED source to the floor, H_{S}	3m
Radiation radius of LED source, r_{S}	6m
Transmitting power of LED source, P_{S}	6W
Height from the relay to the floor, H_{R}	2m
Radiation radius of the relay, r_{R}	3m
Transmitting power of the relay, P_{R}	2W
LED semi-angle, $\theta_{1/2,i,j}$	70^{o}
Field of view of the receiver PD, $\Psi_{i,j}$	90^{o}
Noise variance, $\mathcal{N}_{i,j}$	-98.82dBm
Refractive index, $n_{i,j}$	1.0
Security capacity threshold, C_{th}	1bit/s/Hz

The whole link is connected in the relay-aided VLC system only under the condition that both SR and RU links are connected. Otherwise, the relay-aided VLC system occurs outage. Thus, the upper and lower bounds of the SOP in the DF relay-aided VLC system can be respectively given as

$$P_{\mathrm{SOP}}^{\mathrm{R,u}} = 1 - \left(1 - P_{\mathrm{SOP}}^{\mathrm{SR,u}}\right)\left(1 - P_{\mathrm{SOP}}^{\mathrm{RU,u}}\right), \tag{23a}$$

$$P_{\mathrm{SOP}}^{\mathrm{R,l}} = 1 - \left(1 - P_{\mathrm{SOP}}^{\mathrm{SR,l}}\right)\left(1 - P_{\mathrm{SOP}}^{\mathrm{RU,l}}\right). \tag{23b}$$

From the above derivation procedure on the SOP of the relay-aided VLC system, it can be seen that the most complicated calculation on the SOP is for case 4. We introduce the hypergeometric function to tackle the high calculation complication of the integral items in case 4. Moreover, the upper and lower bounds of the SOP are mainly effected by the upper and lower bounds of the security capacity.

For comparison, similar to the upper and lower bounds of the SOP in the DF relay-aided VLC system, the upper and lower bounds of the SOP in the non-relay VLC system can be respectively derived as

$$P_{\mathrm{SOP}}^{\mathrm{u}} = P_{\mathrm{SOP1}}^{\mathrm{SU}}(\sigma_{\mathrm{u}}, \zeta_{\mathrm{u}}) + P_{\mathrm{SOP2}}^{\mathrm{SU}}(\sigma_{\mathrm{u}}, \zeta_{\mathrm{u}}) + P_{\mathrm{SOP4}}^{\mathrm{SU}}(\sigma_{\mathrm{u}}, \zeta_{\mathrm{u}}), \tag{24a}$$

$$P_{\mathrm{SOP}}^{\mathrm{l}} = P_{\mathrm{SOP1}}^{\mathrm{SU}}(\sigma_{\mathrm{l}}, \zeta_{\mathrm{l}}) + P_{\mathrm{SOP2}}^{\mathrm{SU}}(\sigma_{\mathrm{l}}, \zeta_{\mathrm{l}}) + P_{\mathrm{SOP4}}^{\mathrm{SU}}(\sigma_{\mathrm{l}}, \zeta_{\mathrm{l}}). \tag{24b}$$

where the superscript SU denotes the direct transmission link between the LED source and the legitimate user in the non-relay VLC system.

IV. SIMULATION RESULTS AND DISCUSSION

In this section, numerical simulation results are presented to validate the correctness of the derived theoretical expressions of the upper and lower bounds of the SOP in the DF relay-aided VLC system based on Monte Carlo simulation. Moreover, the impact factors on the SOP in the DF relay-aided VLC system are analyzed from the eavesdroppers' distribution density, the radiation radius of LED source, the radiation radius and deployment height of the relay.

In the simulation, the corresponding parameters are set as follows. It is assumed that there are a LED source, a LED-PD relay, a legitimate user and multiple randomly distributed eavesdroppers in the considered DF relay-aided VLC system. Similar to the works in [17] and [20], if not specified, the simulation parameters are summarized in Table I.

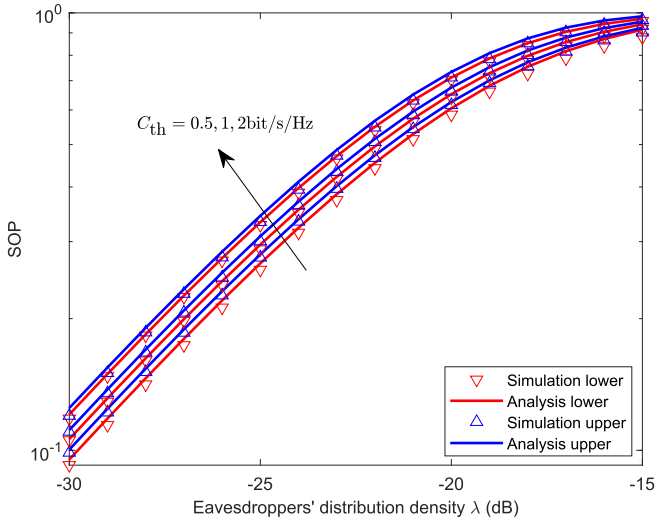

Fig. 2. The SOP of the DF relay-aided VLC system versus the eavesdroppers' distribution density for various security capacity thresholds.

Fig. 2 presents the SOP of the DF relay-aided VLC system versus the eavesdroppers' distribution density for various security capacity thresholds. It can be observed that the theoretical analysis results are consistent with the simulation results of the upper and lower bounds of the SOP for various security capacity thresholds. It verifies the accuracy of the derived theoretical analysis results by employing the hypergeometric function. Moreover, it can be seen that the gap between the upper bound and the lower bound is tight. Furthermore, it can be observed that the upper and lower bounds of the SOP increase with the eavesdroppers' distribution density and the security capacity threshold, i.e., the PLS performance of the DF relay-aided VLC system decreases with the eavesdroppers' distribution density and the security capacity threshold increase. This reason is that the probability of being eavesdropped for the SR and RU links increases with the eavesdroppers' distribution density and the security capacity threshold.

Fig. 3(a) shows the SOP versus the eavesdroppers' distribution density for the DF relay-aided VLC system and the non-relay VLC system. It can be observed that the PLS performance in the DF relay-aided VLC system is deteriorated compared with the non-relay VLC system. This indicates that the relay-aided VLC system is faced with greater PLS risk when the relay node is introduced to extend the scope of communication services and improve the system outage performance. There are two main reasons. On one hand, the node number of being eavesdropped increases in the DF relay-aided VLC system compared with the non-relay system. On the other hand, the channel quality between the relay and eavesdroppers is also improved when the channel quality between the relay and the legitimate user is enhanced. Thus, some measures need to be taken to enhance the PLS performance for the DF relay-aided VLC system. For example, encryption algorithm or coding technology can be introduced to encrypt signals. Besides, the relay can be also chosen as the active interference source to interfere with the

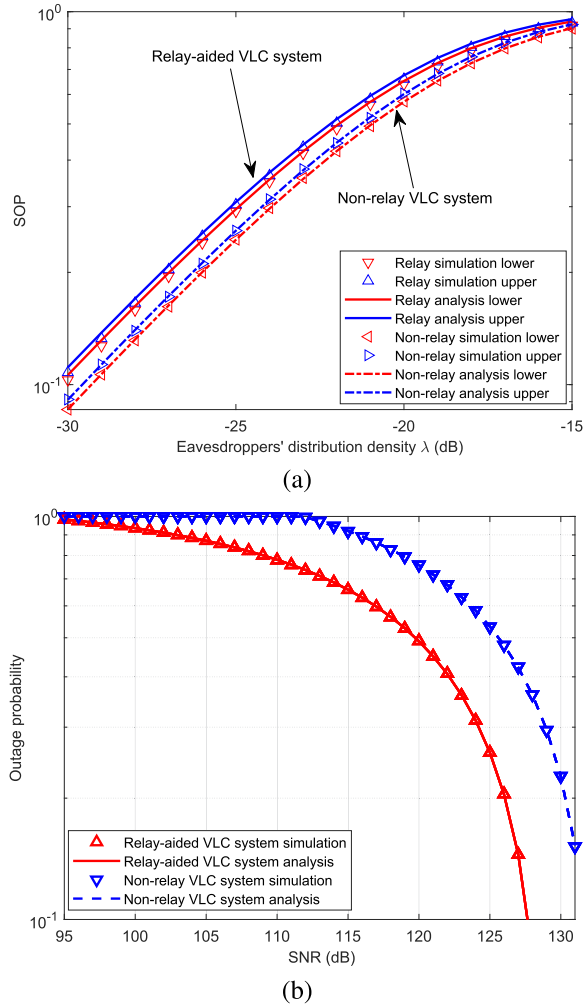

Fig. 3. The SOP and the outage probability for the DF relay-aided VLC system and the non-relay VLC system: (a) the SOP versus the eavesdroppers' distribution density, (b) the outage probability versus SNR of the transmitted signal.

eavesdroppers. By employing the above schemes, it is more difficult for transmission signals to be deciphered by eavesdroppers. Although the relay node increases the secure risk, the relay can effectively improve the quality of communication services for cell-edge users. Specifically, it can be seen from Fig. 3(b) that the outage performance of the relay-aided VLC system is obviously superior to the non-relay VLC system.

Fig. 4 shows the SOP of the DF relay-aided VLC system versus the eavesdroppers' distribution density for various radiation radiuses of the LED source. It can be seen that the SOP of the DF relay-aided VLC system increases with the radiation radius of the LED source. In other words, the PLS performance decreases with the radiation radius of the LED source increase in the DF relay-aided VLC system. This is because the eavesdroppers' number increases with the radiation radius of the LED source, and the corresponding probability of the SR and RU links being eavesdropped increases in the DF relay-aided VLC system. In addition, the communication range of the LED source increases with the radiation radius of the LED source. Thus, the radiation

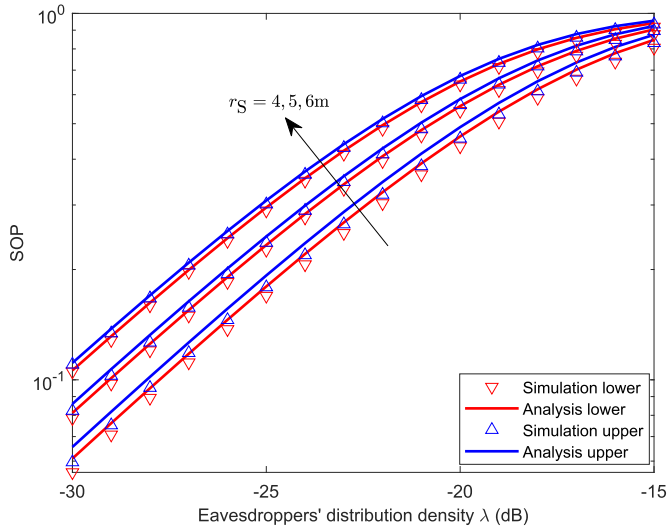

Fig. 4. The SOP of the DF relay-aided VLC system versus the eavesdroppers' distribution density for various radiation radiuses of the LED source.

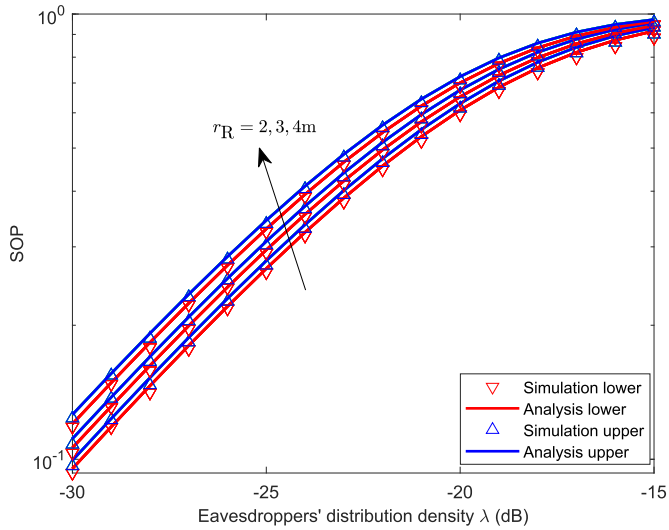

Fig. 5. The SOP of the DF relay-aided VLC system versus the eavesdroppers' distribution density for various radiation radiuses of the relay.

radius of the LED source should be reasonably set up for achieving a balance between the PLS performance and the radiation range of the LED source.

Fig. 5 presents the SOP of the DF relay-aided VLC system versus the eavesdroppers' distribution density for various radiation radiuses of the relay. It can be observed that the SOP of the DF relay-aided VLC system increases with the radiation radius of the relay. Because the eavesdroppers' number distributed within the relay radiating area increases with the radiation radius of the relay, and the corresponding PLS risk of the DF relay-aided VLC system increases. At the same time, the distribution range of the legitimate user increases with the radiation radius of the relay. Thus, the radiation radius of the relay should be reasonably set up to improve the PLS performance and simultaneously provide

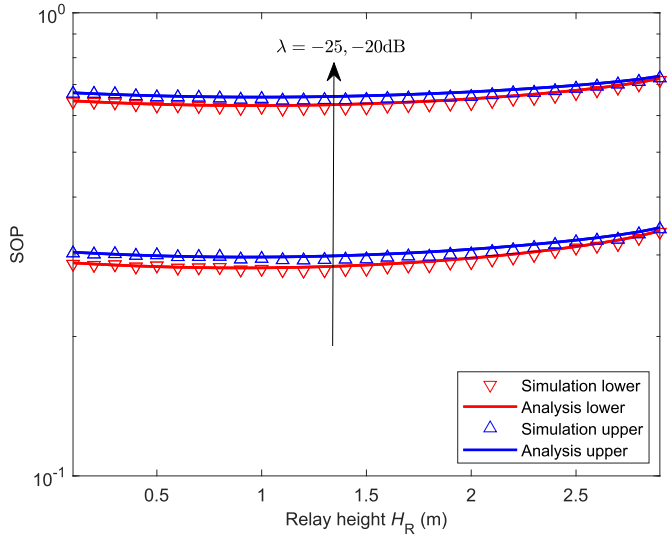

Fig. 6. The SOP of the DF relay-aided VLC system versus the deployment height of the relay for various eavesdroppers' distribution densities.

as wide distribution range as possible for the legitimate user in the DF relay-aided VLC system.

Fig. 6 presents the SOP of the DF relay-aided VLC system versus the deployment height of the relay for various eavesdroppers' distribution densities. It can be observed that the SOP of the DF relay-aided VLC system first slowly decreases and then slowly increases with the deployment height of the relay increase. This reason is mainly as follows. Firstly, the distance between the relay and the eavesdropper increases with the deployment height of the relay, resulting in the probability of being eavesdropped for the SR and RU links decreasing, i.e., the SOP decreases. Secondly, when the deployment height of the relay increases, the channel gain h_{SR} and h_{RU} increases and decreases, respectively. The corresponding SOPs in the SR link and the RU link decreases and increases, respectively. Moreover, the transmission efficiency of the relay diminishes with the deployment height of the relay increase. As a result, the SOP of the RU link increases. To sum up the above cases, the total decreasing of the SOP can compensate for the total increasing. Then, when the deployment height of the relay continues to increase, the received visible light of the relay from the LED source becomes more divergent, and the corresponding SOP in the SR link increases. As a result, the total decreasing of the SOP can not compensate for the total increasing. Therefore, there is an optimal relay deployment height to obtain the optimum security outage performance of the DF relay-aided VLC system.

V. Conclusion

In this paper, the PLS performance of the DF relay-aided VLC system is investigated since the relay-aided VLC system is faced with greater PLS risks. Particularly, the practical deployment characteristic of the relay, the random distribution properties of eavesdroppers and the legitimate user, and the amplitude constraint on transmission signals are taken into account in the DF relay-aided VLC system. The theoretical expressions of the

upper and lower bounds of the SOP in the DF relay-aided VLC system are derived based on the stochastic geometry analysis method. Simulation results verify the correctness of the theoretical expressions of the SOP for the DF relay-aided VLC system. Moreover, it proves the security outage performance of the DF relay-aided VLC system is deteriorated compared with the non-relay VLC system. In addition, it shows the relations between the SOP of the DF relay-aided VLC system and the impact factors from the eavesdroppers' distribution density, the radiation radius of the LED source, the radiation radius and deployment height of the relay. Furthermore, the optimal deployment height of the relay can be determined to obtain the optimum security outage performance of the DF relay-aided VLC system. These parameters can effectively guide the design of the secure relay-aided VLC system.

REFERENCES

[1] X. Wu, M. D. Soltani, L. Zhou, M. Safari, and H. Haas, "Hybrid LiFi and WiFi networks: A survey," *IEEE Commun. Surv. Tut.*, vol. 23, no. 2, pp. 1398–1420, Second quarter 2021.

[2] Q. Wu, W. Chen, D. W. K. Ng, and R. Schober, "Spectral and energy efficient wireless powered IoT networks: NOMA or TDMA?," *IEEE Trans. Veh. Technol.*, vol. 67, no. 7, pp. 6663–6667, Jul. 2018.

[3] A. M. Abdelhady, O. Amin, A. Chaaban, B. Shihada, and M. S. Alouini, "Downlink resource allocation for dynamic TDMA-based VLC systems," *IEEE Trans. Wireless Commun.*, vol. 18, no. 1, pp. 108–120, Jan. 2019.

[4] X. Deng, K. Arulandu, Y. Wu, G. Zhou, and J. P. M. G. Linnartz, "Performance analysis for joint illumination and visible light communication using buck driver," *IEEE Trans. Commun.*, vol. 66, no. 5, pp. 2065–2078, May 2018.

[5] L. Feng, R. Q. Hu, J. Wang, P. Xu, and Y. Qian, "Applying VLC in 5G networks: Architectures and key technologies," *IEEE Netw.*, vol. 30, no. 6, pp. 77–83, Nov./Dec. 2016.

[6] X. Zhu, C. X. Wang, J. Huang, M. Chen, and H. Haas, "A novel 3D non-stationary channel model for 6G indoor visible light communication systems," *IEEE Trans. Wireless Commun.*, vol. 21, no. 10, pp. 8292–8307, Oct. 2022.

[7] A. M. Salhab, A. Chaaban, S. A. Zummo, and M. Alouini, "Power allocation and link selection for multicell cooperative NOMA hybrid VLC/RF systems," *IEEE Commun. Lett.*, vol. 25, no. 2, pp. 560–564, Feb. 2021.

[8] X. Zhang, Y. Zhang, Z. Yan, J. Xing, and W. Wang, "Performance analysis of cognitive relay networks over Nakagami-m fading channels," *IEEE J. Sel. Areas Commun.*, vol. 33, no. 5, pp. 865–877, May 2015.

[9] A. Jee, K. Agrawal, and S. Prakriya, "A coordinated direct AF/DF relay-aided NOMA framework for low outage," *IEEE Trans. Commun.*, vol. 70, no. 3, pp. 1559–1579, Mar. 2022.

[10] R. C. Kizilirmak, O. Narmanlioglu, and M. Uysal, "Relay-assisted OFDM-based visible light communications," *IEEE Trans. Commun.*, vol. 63, no. 10, pp. 3765–3778, Oct. 2015.

[11] L. Feng, R. Q. Hu, J. Wang, and Y. Qian, "Deployment issues and performance study in a relay-assisted indoor visible light communication system," *IEEE Syst. J.*, vol. 13, no. 1, pp. 562–670, Mar. 2019.

[12] Y. Hong, L. K. Chen, and J. Zhao, "Channel-aware adaptive physical-layer network coding over relay-assisted OFDM-VLC networks," *J. Lightw. Technol.*, vol. 38, no. 6, pp. 1168–1177, Mar. 2020.

[13] Y. Xiao, P. D. Diamantoulakis, Z. Fang, Z. Ma, L. Hao, and G. K. Karagiannidis, "Hybrid lightwave/RF cooperative NOMA networks," *IEEE Trans. Wireless Commun.*, vol. 19, no. 2, pp. 1154–1166, Feb. 2020.

[14] M. Zhu, Y. Wang, X. Liu, S. Ma, X. Zhang, and Y. Fu, "Performance analysis for DF relay-aided visible light communication system with NOMA," *IEEE Photon. J.*, vol. 14, no. 5, Oct. 2022, Art. no. 7350809.

[15] A. Mostafa and L. Lampe, "Physical-layer security for MISO visible light communication channels," *IEEE J. Sel. Areas Commun.*, vol. 33, no. 9, pp. 1806–1818, Sep. 2015.

[16] G. Pan, J. Ye, and Z. Ding, "On secure VLC systems with spatially random terminals," *IEEE Commun. Lett.*, vol. 21, no. 3, pp. 492–495, Mar. 2017.

[17] X. Liu, Y. Wang, F. Zhou, Z. Deng, and R. Q. Hu, "Performance analysis on visible light communications with multi-eavesdroppers and practical amplitude constraint," *IEEE Commun. Lett.*, vol. 23, no. 12, pp. 2292–2295, Dec. 2019.

[18] F. Yang, J. Wang, and Y. Dong, "Physical-layer security for indoor VLC wiretap systems under multipath reflections," *IEEE Trans. Wireless Commun.*, vol. 21, no. 12, pp. 11179–11192, Dec. 2022.

[19] Z. Liao, L. Yang, J. Chen, H. C. Yang, and M. S. Alouini, "Physical layer security for dual-hop VLC/RF communication systems," *IEEE Commun. Lett.*, vol. 22, no. 12, pp. 2603–2606, Dec. 2018.

[20] G. Pan et al., "Secure cooperative hybrid VLC-RF systems," *IEEE Trans. Wireless Commun.*, vol. 19, no. 11, pp. 7097–7107, Nov. 2020.

[21] A. Kumar, P. Garg, and A. Gupta, "PLS analysis in an indoor heterogeneous VLC/RF network based on known and unknown CSI," *IEEE Syst. J.*, vol. 15, no. 1, pp. 68–76, Mar. 2021.

[22] S. Ma, Y. He, H. Li, S. Lu, F. Zhang, and S. Li, "Optimal power allocation for mobile users in non-orthogonal multiple access visible light communication networks," *IEEE Trans. Commun.*, vol. 67, no. 3, pp. 2233–2244, Mar. 2019.

[23] A. Arafa, E. Panayirci, and H. V. Poor, "Relay-aided secure broadcasting for visible light communications," *IEEE Trans. Commun.*, vol. 67, no. 6, pp. 4227–4239, Jun. 2019.

[24] S. Cho, G. Chen, and J. P. Coon, "Securing visible light communication systems by beamforming in the presence of randomly distributed eavesdroppers," *IEEE Trans. Wireless Commun.*, vol. 17, no. 5, pp. 2918–2931, May 2018.

[25] L. Yin, W. O. Popoola, X. Wu, and H. Haas, "Performance evaluation of non-orthogonal multiple access in visible light communication," *IEEE Trans. Commun.*, vol. 64, no. 12, pp. 5162–5175, Dec. 2016.

[26] J. M. Kahn and J. R. Barry, "Wireless infrared communications," *Proc. IEEE*, vol. 85, no. 2, pp. 265–298, Feb. 1997.

[27] X. Liu, Z. Chen, Y. Wang, F. Zhou, and S. Ma, "Robust artificial noise-aided beamforming for a secure MISO-NOMA visible light communication system," *China Commun.*, vol. 17, no. 11, pp. 42–53, Nov. 2020.

[28] Y. Guo, K. Xiong, Y. Lu, D. Wang, and K. B. Letaief, "Achievable information rate in hybrid VLC-RF networks with lighting energy harvesting," *IEEE Trans. Wireless Commun.*, vol. 69, no. 10, pp. 6852–6864, Oct. 2021.

[29] X. Li, J. Li, and L. Li, "Performance analysis of impaired SWIPT NOMA relaying networks over imperfect Weibull channels," *IEEE Syst. J.*, vol. 14, no. 1, pp. 669–672, Mar. 2020.

[30] B. Westcott, "Generalized confluent hypergeometric and hypergeometric transmission lines," *IEEE Trans. Circuit Theory*, vol. 16, no. 3, pp. 289–294, Aug. 1969.